A DNS study of detonation-turbulence interaction using massless tracer particles: effects of turbulent Reynolds number

Sou Suzuki[a,*], Kazuya Iwata[a], Reo Kai[b], and Ryoichi Kurose[a]

[a]Department of Mechanical Engineering and Science, Kyoto University,
Kyoto daigaku-Katsura,Nishikyo-ku, Kyoto 615-8540, Japan

[b]Faculty of Engineering Sciences, Kyushu University,
Kasuga, Fukuoka 816-8580, Japan

1 Introduction

Detonation-turbulence interaction is an important factor in understanding the phenomena occurring in the detonation engines. However, there are only a few studies about the effects of turbulent flow on the detonation waves. Jin et al.[1] conducted three-dimensional Direct Numerical Simulations (DNS) to investigate the effects of turbulence on the detonation front and downstream turbulent characteristics. Because they adopted the single-step simple chemistries, they cannot capture the actual physics of detonations including many chemical species. Iwata et al.[2] conducted three-dimensional DNSs with the detailed reaction mechanism for the detonations propagating in the stoichiometric hydrogen/oxygen mixture diluted by argon. They deduced that turbulence promotes the post-shock reactions and changes the distributions of incident shock Mach number. Suzuki et al.[3] performed three-dimensional DNSs that detonations propagate in non-diluted stoichiometric hydrogen/oxygen mixtures under multi-intensity turbulent fields represented by the turbulent Mach numbers. They concluded that strong turbulence destroys the regular detonation structures and extremely strong turbulence makes the peak pressure low. In those studies, the temporal- and spatial-averaging smooths out the peaky profiles of detonation structure. In addition, the effects of turbulent Reynolds numbers have not been examined.

Therefore, the objective of this study is to analyze the effects of turbulent velocity fields represented by the turbulent Reynolds numbers. Particularly, three-dimensional DNSs with tracer particles are conducted for the detonation propagating in the non-diluted stoichiometric hydrogen/oxygen with and without turbulence.

2 Direct Numerical Simulation

The governing equations in this study are three-dimensional compressible Navier-Stokes equations, transport equations for 8 species involved in hydrogen-oxygen combustion, and the equation of state for ideal gas. The detailed reaction mechanism proposed and validated by Conaire

Correspondence to: suzuki.sou.48s@st.kyoto-u.ac.jp

Table 1: Summary of explored turbulent conditions.

Re_λ	Ma_t	L [µm]	λ [µm]	η [µm]	u_{rms} [m/s]	u_d [m/s]	u_s [m/s]
-	-	-	-	-	-	-	-
140	0.51	61.8	48	2.08	274	34	272
250	0.51	110	86	2.78	273	28	272
360	0.51	159	125	3.37	271	29	269

et al.[4] is used as done in our previous work[3]. Massless tracer particles are set up as non-inertial Lagrangian particles. They move following the local fluid velocity and the flow properties such as temperature and pressure are recorded every 2 steps on each particle position.

The in-house CFD code FK^3[2, 3, 5], which has been developed at Kyoto University, is used in this study. The same numerical methods are applied as in our previous work[3]. Reconstruction is implemented by fifth-order WENO[6], convective fluxes are by Lax-Fridrich or HLLC methods, time integrations for the flow are by third-order TVD Runge-Kutta, and time integrations for chemical reactions are by the Dual-Time stepping methods.

The computational domain is the same the one in our previous work[3]. The size of the rectangular is L=2.40 mm(x)× W=3.84 mm(y)× H=3.84 mm(z), which is divided by rectangular cells of 2 µm(x)× 4 µm(y)× 4 µm(z). The total grid number is 1200× 960× 960 ≈, 1.1 billion grids. Boundary conditions are implemented in the same way as our previous work[3]; periodic boundaries are set in the y- and z-directions, the outflow is NSCBC, and the inflow velocity is balanced to the detonation velocity. Detonation waves are thereby fixed within a few grids in the domain.

The inflow turbulences are specified by the parameters as the turbulent Reynolds number Re_λ=$\rho u_{rms}\lambda/\mu$ and the turbulent Mach number $\mathrm{Ma_t}$=u_{rms}/c defined in [7, 8]. ρ, u_{rms}, λ, μ, and c indicate the density, root mean square (rms) of velocity, Taylor micro-scale, viscosity, and sound speed. The dilatational and solenoidal components of velocities are u_d and u_s calculated by Helmholtz decomposition. In this study, one case is simulated without turbulence and three cases are done with turbulences specified by 3 turbulent Reynolds numbers of Re_λ=140, 250, and 360. Turbulent Mach number $\mathrm{Ma_t}$ is set to be 0.51 because the change of cell structure was observed in [3]. The investigated turbulence conditions are summarized in Table 1. In all cases, the initial pressure and temperature are 40 kPa and 295 K. The inflow mixture is the stoichiometric hydrogen/oxygen.

3 Results and Discussion

Figure 1 shows the instantaneous three-dimensional detonation structures. Shock front is represented as an iso-surface of p = 250 kPa and flame front as an iso-surface of $Y_{\mathrm{H_2}} = Y_{\mathrm{H_2,half}}$ (red surface). Here, p is the pressure and $Y_{\mathrm{H_2}}$ is the mass fraction of $\mathrm{H_2}$. $Y_{\mathrm{H_2,half}}$ indicates the half value of unburnt $Y_{\mathrm{H_2}}$. Density colormap is shown on y = 0 mm and z = 0 mm. Massless tracer particles are shown by white spheres.

In the non-turbulent case, the detonation has the regular and periodic structure including four transverse waves propagating in y- and z-directions. On the other hand, it can be seen that the $\mathrm{Ma_t}$ = 0.51 turbulences destroy the regular detonation structures and corrugate the shocks and flame fronts. Additionally, the flame front gets closer to the shock surface. At smaller Re_λ = 140 case, the corrugations on the shock and flame are smaller than those of Re_λ = 360 case.

The scales of distortions are small at a small turbulent Reynolds number because the vortices are small. Those results are consistent with our previous work[3].

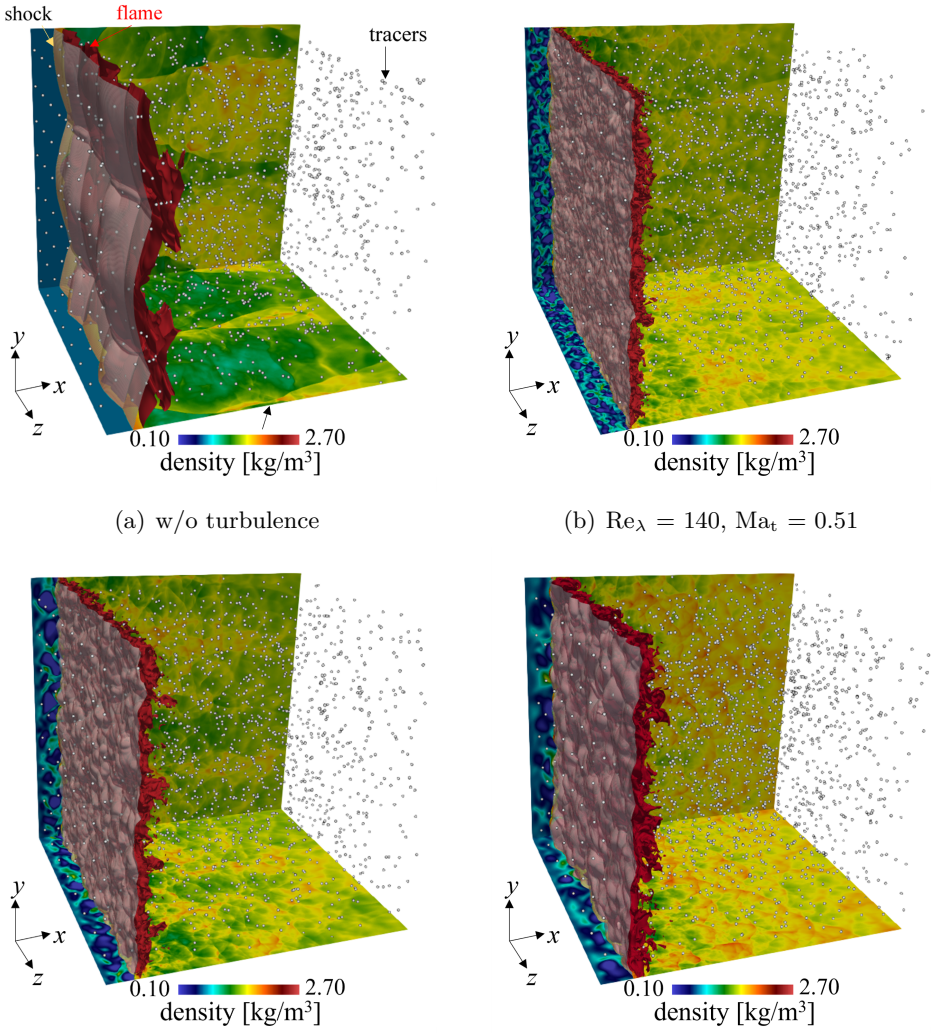

(a) w/o turbulence

(b) $\mathrm{Re}_\lambda = 140$, $\mathrm{Ma}_\mathrm{t} = 0.51$

(c) $\mathrm{Re}_\lambda = 250$, $\mathrm{Ma}_\mathrm{t} = 0.51$

(d) $\mathrm{Re}_\lambda = 360$, $\mathrm{Ma}_\mathrm{t} = 0.51$

Figure 1: Instantaneous 3D structure of detonation: shock front is represented as an iso-surface of p=250 kPa (translucent gray surface) and flame front as an iso-surface of $Y_{\mathrm{H_2}} = Y_{\mathrm{H_2,half}}$ (red surface). Density colormap is shown on $y = 0$ mm and $z = 0$ mm. Massless tracer particles are described by white spheres.

Figure 2(a) shows the mass fractions of major species as H_2, O_2, and H_2O represented as blue, red, and light blue lines, respectively. Fig. 2(b) shows the mass fractions of minor species as OH, H, and HO_2 represented as black, red, and green lines. These statistical values are obtained from the ensemble averaging of values recorded by tracers along their moving paths. In the non-turbulent case denoted by solid lines, the fuel H_2 and the oxidizer O_2 decrease the slowest in this study. The effects of turbulence that promote reactions are consistent with our previous work[3]. Minor species increase more rapidly at smaller Re_λ coincident with the increased production of H_2O. As the chemical reaction is promoted, HO_2 mass fraction increases. This corresponds to our previous work[3], and is clearer in this study. Therefore, the increased minor species lead to rapid reaction progress. The chemical reactions progress the fastest in the Re_λ

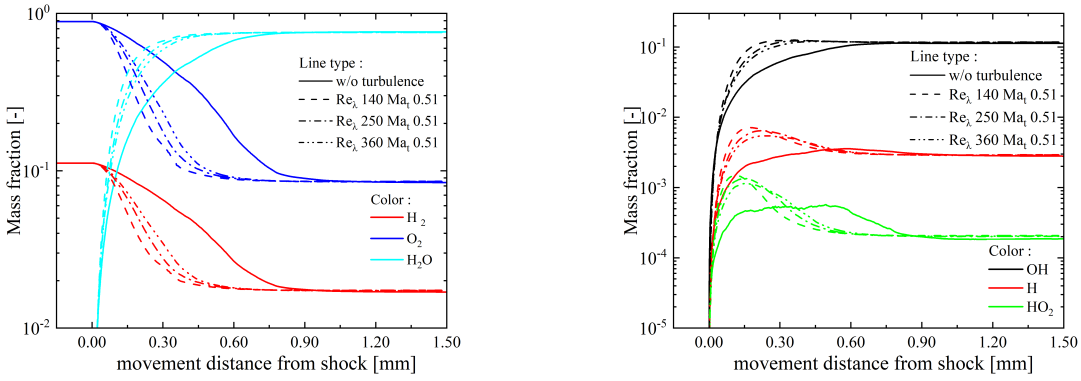

(a) Major species (b) Minor species

Figure 2: Ensemble averaged profiles of mass fractions recorded by tracers along their moving path.

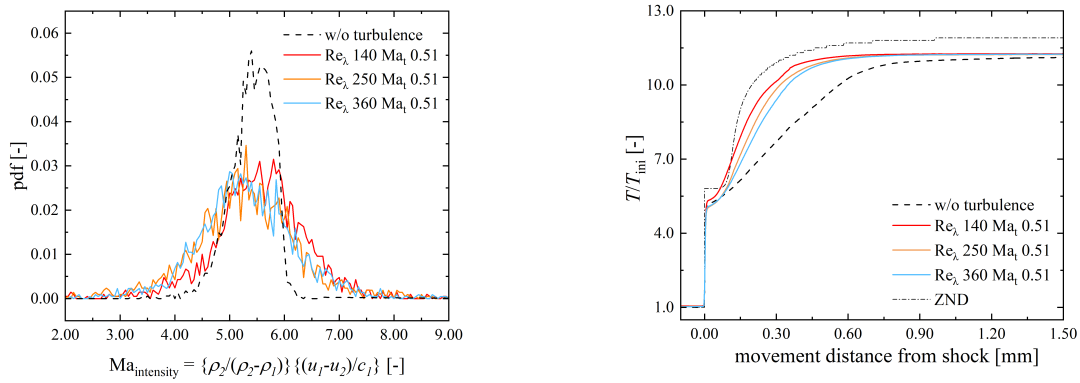

(a) pdf of shock intensity (b) Temperature

Figure 3: Probability density functions (pdf) of shock intensity and ensemble-averaged profiles of normalized temperature recorded by tracers along their moving path.

= 140 case. In the figure, the turbulence with smaller turbulent Reynolds numbers promotes the reactions and rapidly reaches equilibrium.

Figure 3 shows the probability density function (pdf) of the shock intensity and the ensemble-averaged profiles of normalized temperature, both of them are recorded by tracers. Shock intensity represents the relative velocity across the shock, which is the indicator of shock compression[9]. In the figure, the non-turbulent case is denoted by a black dashed line and turbulent cases are by colored lines. One of the turbulent effects on the detonation that can be seen here is to change the shock intensity. The shock intensity is defined as $\mathrm{Ma}_{\mathrm{intensity}} = \{\rho_2/(\rho_2-\rho_1)\}\{(u_1-u_2)/c_1\}$. Subscripts 1 and 2 indicate the pre- and post-shock state, respectively. It is derived from the assumption that the local shock crossed by tracers is regarded as a steady shock wave. In this study, the shock intensity Mach number is calculated according to this equation using the above parameters recorded by each tracer when they pass across the shock. In Fig. 3(a), the distribution is broader than in the non-turbulent case. The distributions are similar in the $\mathrm{Re}_\lambda = 250$ and 360 cases, and are higher in the $\mathrm{Re}_\lambda = 140$ case. Therefore, it is implied that the difference in shock intensity distributions affects the reaction progress. Fig. 3(b) shows that temperature downstream the shock increases with the reaction progress. On

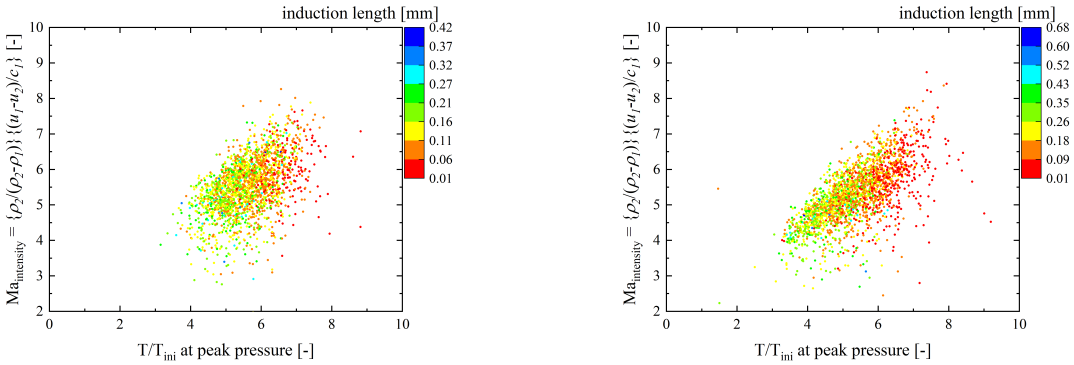

(a) $\mathrm{Re}_\lambda = 140$ (b) $\mathrm{Re}_\lambda = 360$

Figure 4: Scatter plots of the normalized temperature T/T_{ini} at peak pressure and the shock intensity $\mathrm{Ma}_{\mathrm{intensity}}$ colored by induction length: recorded by tracers.

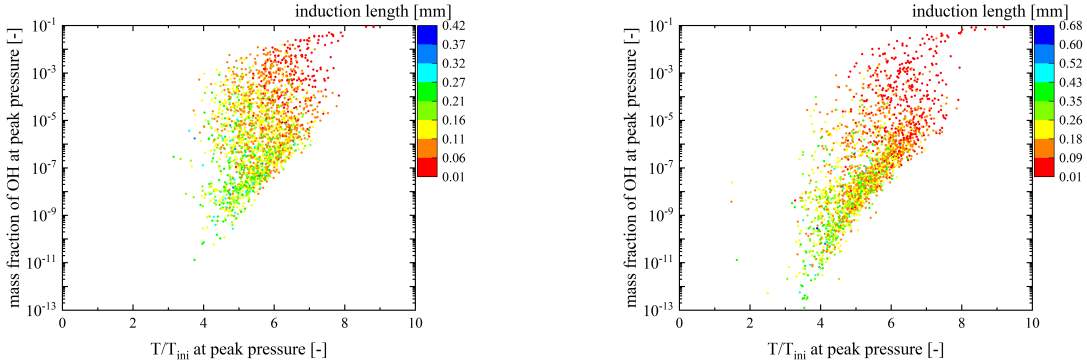

(a) $\mathrm{Re}_\lambda = 140$ (b) $\mathrm{Re}_\lambda = 360$

Figure 5: Scatter plots of the normalized temperature T/T_{ini} and OH mass fractions at peak pressure colored by induction length.

the other hand, the temperature behind the shock is determined by the shock intensity. As the shock intensity becomes higher, the temperature at the position of peak pressure gets higher. In the following, a detailed analysis of temperature using tracers is performed.

Figure 4 shows the scatter plots of the normalized temperature at peak pressure and the shock intensity recorded by tracers, which are colored by the induction lengths. Here, temperature T is normalized by its unburnt value. The induction length is defined as the distance from the shock to the position at which H_2 is half consumed along the tracer moving path. The figure shows that the temperature is proportional to the shock intensity. The points in the high-temperature regions are red, indicating short induction length with enhanced reaction. In the $\mathrm{Re}_\lambda = 140$ case, there are fewer points around $T/T_{ini} = 4.0$ than in the larger turbulent Reynolds number case. The results in the $\mathrm{Re}_\lambda = 250$ case showed the intermedial state between in the $\mathrm{Re}_\lambda = 140$ and 360 cases. It indicates that the turbulence including small eddies increases the temperature.

Figure 5 shows the scatter plots of the normalized temperature and OH mass fractions at peak pressure colored by the induction length. Since OH is an indicator representing the reaction progress, it is selected. The OH mass fractions are relatively proportional to the temperature. In this figure, the distribution shifts to the region where OH mass fraction is high

as the turbulent Reynolds number gets smaller because the tracers recording a high-temperature increase. The points in the high OH region indicate the short induction length. Therefore, the high shock intensity increases the temperature behind the shock. As the temperature is high, more intermediate products are generated, enhancing the reaction progress.

Although not shown here, the shock intensity affects not only the temperature but also the pressure behind the shock. However, the pressures did not correlate to the shock intensity and the induction length because the pressure distribution is more sensitive to subsequent compression/expansion flow to smooth it.

4 Conclusion

In this study, the DNSs of detonation-turbulence interaction in a hydrogen/oxygen mixture with massless tracer particles were conducted to investigate the effects of the turbulent Reynolds number.

The non-turbulent detonation is structured regularly and periodically, whereas the turbulence destroys the regular structures. The profiles along the tracer moving path indicated that the chemical reactions progressed rapidly in the smaller turbulent Reynolds number turbulence cases, which are similar to the results of temperatures. Using the tracers, it is indicated the shock intensities coincide with the temperature distributions behind the shock. In the smaller turbulent Reynolds number turbulence, the high shock intensity increases the temperature. As the temperature becomes higher, more intermediate products such as OH are generated. They contribute to the reaction progress, thus the chemical reactions are enhanced in the smaller turbulent Reynolds number cases.

Acknowledgements

This study used the computational resources of the supercomputer Fugaku provided by the RIKEN Center for Computational Science(Project ID:hp240120). This study was supported by JSPS KAKENHI Grant Number JP23K13146.

References

[1] T. Jin et al., Simulations of cellular detonation interaction with turbulent flows, AIAA Journal 54 (2) (2016) 419–433.

[2] K. Iwata et al., Direct numerical simulation of detonation–turbulence interaction in hydrogen/oxygen/argon mixtures with a detailed chemistry, Physics of Fluids 35 (4) (2023).

[3] S. Suzuki et al., A dns study of detonation in h2/o2 mixture with variable-intensity turbulences, Proceedings of the Combustion Institute 40 (1-4) (2024) 105337.

[4] M. Ó Conaire et al., A comprehensive modeling study of hydrogen oxidation, International journal of chemical kinetics 36 (11) (2004) 603–622.

[5] R. Kurose, About in-house code FK^3., http://www.tse.me.kyoto-u.ac.jp/members/kurose/link_e.php.

[6] G.-S. Jiang, C.-W. Shu, Efficient implementation of weighted eno schemes, Journal of Computational Physics 126 (1) (1996) 202–228.

[7] J. Mathieu, J. Scott, An introduction to turbulent flow, Cambridge University Press, 2000.

[8] J. Larsson et al., Reynolds-and mach-number effects in canonical shock–turbulence interaction, Journal of Fluid Mechanics 717 (2013) 293–321.

[9] P. H. Oosthuizen, W. E. Carscallen, Compressible fluid flow, Vol. 179, McGraw-Hill New York, 1997.